

¹³C-Metabolic Flux Analysis for Batch Culture of *Escherichia coli* and Its *pyk* and *pgi* Gene Knockout Mutants Based on Mass Isotopomer Distribution of Intracellular Metabolites

Yoshihiro Toya

Institute for Advanced Biosciences, Keio University, Tsuruoka 997-0017, Japan

Systems Biology Program, Graduate School of Media and Governance, Keio University, Fujisawa 252-8520, Japan

Nobuyoshi Ishii, Kenji Nakahigashi, and Takashi Hirasawa

Institute for Advanced Biosciences, Keio University, Tsuruoka 997-0017, Japan

Tomoyoshi Soga, and Masaru Tomita

Institute for Advanced Biosciences, Keio University, Tsuruoka 997-0017, Japan

Systems Biology Program, Graduate School of Media and Governance, Keio University, Fujisawa 252-8520, Japan

Kazuyuki Shimizu

Institute for Advanced Biosciences, Keio University, Tsuruoka 997-0017, Japan

Dept. of Bioscience and Bioinformatics, Kyushu Institute of Technology, Iizuka 820-8502, Japan

DOI 10.1002/btpr.420

Published online March 18, 2010 in Wiley Online Library (wileyonlinelibrary.com).

Since most bio-production processes are conducted in a batch or fed-batch manner, the evaluation of metabolism with respect to time is highly desirable. Toward this aim, we applied ¹³C-metabolic flux analysis to nonstationary conditions by measuring the mass isotopomer distribution of intracellular metabolites. We performed our analysis on batch cultures of wild-type *Escherichia coli*, as well as on *Pyk* and *Pgi* mutants, obtained the fluxes and metabolite concentrations as a function of time. Our results for the wild-type indicated that the TCA cycle flux tended to increase during growth on glucose. Following glucose exhaustion, cells controlled the branch ratio between the glyoxylate pathway and the TCA cycle, depending on the availability of acetate. In the *Pyk* mutant, the concentrations of glycolytic intermediates changed drastically over time due to the dumping and feedback inhibition caused by PEP accumulation. Nevertheless, the flux distribution and free amino acid concentrations changed little. The growth rate and the fluxes remained constant in the *Pgi* mutant and the glucose-6-phosphate dehydrogenase reaction was the rate-limiting step. The measured fluxes were compared with those predicted by flux balance analysis using maximization of biomass yield or ATP production. Our findings indicate that the objective function of biosynthesis became less important as time proceeds on glucose in the wild-type, while it remained highly important in the *Pyk* mutant. Furthermore, ATP production was the primary objective function in the *Pgi* mutant. This study demonstrates how cells adjust their metabolism in response to environmental changes and/or genetic perturbations in the batch cultivation. © 2010 American Institute of Chemical Engineers *Biotechnol. Prog.*, 26: 975–992, 2010

Keywords: ¹³C-metabolic flux analysis, batch culture, *Escherichia coli*, *Pyk* mutant, *Pgi* mutant

Introduction

Although ¹³C-metabolic flux analysis (¹³C-MFA) is a powerful approach for estimating intracellular metabolic fluxes,^{1–3} the conventional ¹³C-MFA method, based on isotope labeling patterns of proteinogenic amino acids, cannot be applied to industrially important batch or fed-batch cultures in nature.⁴ The reason for this limitation is that the isotope labeling patterns of the proteinogenic amino acids

Additional Supporting Information may be found in the online version of this article

Current address of Takashi Hirasawa: Dept. of Bioinformatic Engineering, Graduate School of Information Science and Technology, Osaka University, Suita 565-0871, Japan.

Correspondence concerning this article should be addressed to K. Shimizu at shimi@bio.kyutech.ac.jp.

sampled at any given time are composed of all past labeling information, up to the moment of sampling. Therefore, most conventional ^{13}C -MFA has been conducted in continuous cultures. However, batch culture, in which the state variables such as the number of cells and the extracellular and intracellular metabolite concentrations vary with respect to time, is often employed in the fermentation industry. Although the cell growth phase is of primary importance, many useful metabolites are produced in the stationary phase.⁵ Thus, the establishment of an effective method for evaluation of the metabolic fluxes with respect to time as the culture environment changes is a very desirable goal.

Recently, the application of ^{13}C -MFA to the nonstationary state has attracted a great deal of attention. To apply ^{13}C -MFA to the nonstationary state, Antoniewicz et al. introduced two theoretical parameters, the fractional contribution of the feed to the production of labeled products and the fraction of labeled products in the sample, as compensatory parameters to account for the isotopic transients.⁶ These parameters facilitate the determination of metabolic fluxes in fed-batch cultures of *Escherichia coli* producing 1,3-propanediol, based on the mass isotopomer distributions of the proteinogenic amino acids obtained by GC-MS. Iwatani et al. introduced a parameter for the effect of protein turnover and performed ^{13}C -MFA using the mass isotopomer distributions of intracellular amino acids measured by LC-MS/MS in a fed-batch culture of *E. coli*.⁷ A more straightforward approach would involve measuring the mass isotopomer distributions of intermediate metabolites. The pool sizes of these compounds are much smaller than those of proteinogenic amino acids, and changes in metabolic fluxes are rapidly reflected in the labeling patterns of the intracellular metabolites.⁸ Thus, as long as the isotopic quasi steady-states of intermediate metabolites are achieved at each sampling point, the ^{13}C -MFA approach can be extended to the nonstationary state in batch or fed-batch cultures. Some recent studies have directly measured the mass isotopomer distributions of intermediate metabolites^{9–11} and simulated the dynamics of the isotopomers.¹² Of particular interest are several studies that have been performed on nonstationary state cells. Nöh et al. conducted isotopically nonstationary ^{13}C -labeling experiments and measured the mass isotopomer distributions of intermediate metabolites using LC-MS/MS. Their approach made it possible to determine a short time response (within 16 seconds).⁸ In addition, they simulated the rapid dynamic behavior of isotopomers in fed-batch cultures in which the fluxes were assumed to be constant during the period of interest. Costenoble et al. also performed ^{13}C -MFA on a fed-batch culture of *Saccharomyces cerevisiae* and analyzed the dynamic changes for the cell cycle.¹³

In this study, we used capillary electrophoresis time-of-flight mass spectrometry (CE-TOFMS) to estimate the flux changes, as well as to measure the changes in metabolite concentrations, in a batch culture environment. CE-TOFMS analysis is a metabolomics technique that allows the simultaneous measurement of many charged, low-molecular-weight metabolites in a high-throughput fashion.^{14,15} Previous study has applied ^{13}C -MFA, based on the mass isotopomer distributions of intermediate metabolites measured by CE-TOFMS, to the examination of steady-state in continuous cultures of *E. coli*.¹⁶

To improve the productivity of the useful compounds, it is important not only to modify the biosynthetic reactions and pathway, but also to control the whole metabolism. There-

fore, it is necessary to understand the regulatory mechanism of the central metabolism, and the analyses of metabolic changes in response to specific gene knockouts provide valuable information for it. The metabolic flux analyses have already been performed for phosphoglucose isomerase (Pgi) and pyruvate kinase (Pyk) mutants in the continuous culture, and it has been reported that the knockout of *pgi* gene caused the activation of the Entner-Doudoroff (ED) pathway and the glyoxylate pathway to alleviate the overproduced NADPH.¹⁷ The knockout of *pyk* gene caused the activation of the anaplerotic reaction Ppc and the depression of Pfk by the accumulated PEP.¹⁸ In Pgi mutant, NADPH is overproduced, and thus the relevance of this mutation is recognized for its application to poly(3-hydroxybutyrate) production, propanol fermentation, heterologous protein production etc., where NADPH availability limits their production rates. In Pyk mutant, its application to aromatic amino acid fermentation may be considered since the aromatic amino acid biosynthetic enzymes were significantly up-regulated, probably caused by the increase in PEP and E4P concentrations.¹⁹ Moreover, Pyk mutant may be applied to succinate and lysine fermentation, since OAA tends to be accumulated through increased Ppc flux.

Although the Pgi and Pyk mutants have the potentials for the bio-productions as stated above, the time-dependent changes of intermediate concentrations and metabolic fluxes have not yet been investigated in the industrially important batch cultures. Although most of the investigations on ^{13}C -MFA have been conducted in the continuous cultures, the glucose concentration in culture medium is low and constant in the continuous culture, which is different from the batch cultures, where the physiology changes with respect to time. In this study, we extended ^{13}C -MFA to the batch cultures to obtain deeper insight into the dynamic metabolic changes that occur in wild-type, Pyk and Pgi mutants. Additionally, by employing FBA with appropriate objective functions, we analyzed how the cell's strategy changes with respect to time.

Materials and Methods

Strains and culture conditions

The strains used were wild-type *E. coli* BW25113 (*lacI^rrrnB_{T14} ΔlacZ_{WJ16}hsdR514 ΔaraBAD_{AH33} ΔrhaBAD_{LD78}*), as well as Pyk and Pgi mutants of the same background strain. The Pyk mutant was constructed using P1-phage-mediated transduction of *pykF::kan*²⁰ with BW25113 carrying *pykA::cat*, which was constructed using the method of Datsenko and Wanner.²¹ Batch and continuous cultivations were performed using synthetic medium (48 mM Na_2HPO_4 , 22 mM KH_2PO_4 , 10 mM NaCl, 45 mM $(\text{NH}_4)_2\text{SO}_4$, 4 g/L glucose) supplemented with 1 mM MgSO_4 , 1 mg/mL thiamine, 0.056 mg/L CaCl_2 , 0.08 mg/L FeCl_3 , 0.01 mg/L $\text{MnCl}_2 \cdot 4\text{H}_2\text{O}$, 0.017 mg/L ZnCl_2 , 0.0043 mg/L $\text{CuCl}_2 \cdot 2\text{H}_2\text{O}$, 0.006 mg/L $\text{CoCl}_2 \cdot 2\text{H}_2\text{O}$, and 0.06 mg/L $\text{Na}_2\text{MoO}_4 \cdot 2\text{H}_2\text{O}$. Continuous cultivation of the wild-type strain was carried out at 37°C in a working volume of 1 L in a 2 L reactor (BMJ02-PI, Able, Tokyo, Japan) equipped with pH, dissolved oxygen, and temperature sensors. The concentrations of O_2 and CO_2 in the off-gas were monitored using an off-gas analyzer (DEX-2562, Able). The airflow rate was maintained at 1 L/min, and the pH was maintained at 7.0 by automatic addition of HCl or NaOH throughout cultivation. The dilution rate for the continuous culture was 0.5 h^{-1} . Batch cultivations

of the wild-type strain and the Pyk and Pgi mutant strains were performed under the same conditions, with the exception that the working volume of the reactor was changed to 1.2 L.

¹³C-labeling experiments

The ¹³C-labeling experiment was initiated in the continuous culture after five residence times to ensure a steady-state condition. The feeding medium containing 4 g/L of naturally labeled glucose was replaced with the same medium containing 2 g/L (50%) [U-¹³C] glucose and 2 g/L (50%) of naturally labeled glucose. In the batch cultures, a mixture of 1.2 g/L (30%) [1-¹³C] glucose, 0.8 g/L (20%) [U-¹³C] glucose, and 2 g/L (50%) naturally labeled glucose was used as a carbon source. The 1st ¹³C labeled carbon originated from [1-¹³C] glucose is released as CO₂ in the oxidative pentose phosphate (PP) pathway, whereas it is conserved in the glycolysis. Thus, the flux ratio between the PP pathway and glycolysis can be identified by the labeling pattern of the metabolites in the lower part of glycolysis. On the other hand, the [U-¹³C] glucose provides information about the fluxes of the anaplerotic and oxidative pathways in tricarboxylic acid (TCA) cycle.

Measurement of biomass and extracellular metabolites

Dry cell weights were measured via optical density at 600 nm. The optical density of the culture broth was converted to dry cell weight using a previously obtained conversion coefficient (1 OD₆₀₀ = 0.3 g/L). The concentrations of extracellular metabolites, such as glucose and acetate, were measured by enzymatic assay kits (F-kit, Roche Diagnostics, Germany).

CE-TOFMS analysis of intercellular metabolites

Sample preparation was carried out using the modified method described by Ohashi et al. (2007).²² An aliquot of culture broth containing 0.015 g of cells was passed through a 0.45- μ m pore size filter (Millipore). The cells on the filter were washed with 20 mL of Milli-Q water at 37°C and metabolism was stopped by submerging in 4 mL of methanol at 4°C containing 2 μ M 2-(*N*-morpholino)ethanesulfonic acid, 2 μ M trimesate, 2 μ M methionine sulfone and 2 μ M 3-aminopyrrolidine as internal standard. Quantities of 4 mL of chloroform and 1.6 mL of Milli-Q water were added to the solution, which was then fully mixed. The solution was centrifuged at 2,300g for 5 min at 4°C, and the separated methanol layer was filtered by centrifugation through a Millipore 5-kDa cutoff filter to remove high-molecular-weight compounds. The filtrate was lyophilized and then dissolved in 50 μ L of Milli-Q water before CE-TOFMS analysis. CE-TOFMS experiments were performed on an Agilent CE capillary electrophoresis system (Agilent Technologies, Germany) and an Agilent G3250AA LC/MSD TOF system (Agilent Technologies, Palo Alto, CA). The CE-TOFMS conditions used for anionic metabolite analysis have been described elsewhere.^{14,15} All measurements were performed three times.

CE-TOFMS analysis of proteinogenic amino acids

Biomass samples obtained from 5 mL of culture broth were suspended in 3 mL of 6 M HCl and hydrolyzed at

105°C for 16 h. After cooling, the HCl was evaporated on a centrifugal evaporator (CVE-3100, Tokyo Rikakikai, Japan). The dried hydrolysate was resuspended in 1.5 mL of water and filtered through a 0.22- μ m pore size filter (Millipore). Conditions for the CE-TOFMS analysis of cationic metabolites have been described elsewhere.^{14,15} The effect of unlabeled biomass in the inocula was corrected using the method of Fischer and Sauer.²³

GC-MS analysis of the labeling information of extracellular acetate

The supernatant of the culture (resulting from centrifugation at 9,100g for 5 min) was analyzed to determine the labeling patterns of extracellular acetate. GC-MS analysis was carried out to measure the isotopomer distribution using an Agilent 5973C Series GC/MSD (Agilent) equipped with a DB-FFAP column (30 m \times 0.25 mm \times 0.50 μ m, Agilent). An injection volume of 1 μ L was used, with the flow mode in split control. The carrier gas flow rate was set at 1 mL/min. The oven temperature was initially held at 100°C for 5 min. Following this first step, the temperature was raised at a rate of 10°C/min until the temperature reached 250°C. This final temperature was maintained for 12 min.

Calculation of isotopomer distributions of extracellular acetate

To estimate the metabolic fluxes during the stationary phase when acetate was consumed, it was necessary to identify the isotopomer distributions of the extracellular acetate produced by the cell. Four stable carbon isotopomers exist for acetate: CH₃CO₂H (I₀₀), ¹³CH₃CO₂H (I₀₁), CH₃¹³CO₂H (I₁₀), and ¹³CH₃¹³CO₂H (I₁₁). I₀₁ and I₁₀ cannot be distinguished from each other, as they share the same value of 61 for *m/z*. To discriminate between I₀₁ and I₁₀, information regarding the fragment ions of acetate is required. Since acetate cannot be fractionated by CE-TOFMS, GC-MS was used to distinguish I₀₁ from I₁₀, as GC-MS can measure acetate ions as well as the fragment ions [M-CH₃]⁺ and [M-OH]⁺. The [M-CH₃]⁺ fragment ion has two isotopomers with *m/z* values of 45 (derived from I₀₀ and I₀₁) and 46 (derived from I₁₀ and I₁₁). Because the GC-MS fragment ratio is constant, the amount of I₁₁ in the peak of the *m/z* reading at 46 can be calculated from the amount in the peak of the *m/z* reading at 62. The amount of I₁₀ in the peak of the *m/z* reading at 61 can then be determined from the residual of the *m/z* peak at 46 (i.e., I₁₀ in the peak of *m/z* at 46). Because the residual in the peak of *m/z* at 61 measures I₀₁, the ratio between I₀₁ and I₁₀ can then be determined (see Supporting Information Figure S1). We validated that this method could determine the isotopomer distributions of the standard mixture of unlabeled acetate, as well as of [1-¹³C] and [2-¹³C] sodium acetates (Wako Co., Osaka, Japan).

¹³C-Metabolic flux analysis

Stoichiometric reaction models were constructed for ¹³C-MFA. The model for glucose consumption in the batch culture consisted of glycolysis, the PP pathway, the TCA cycle, and the anaplerotic pathway. The ED pathway and the glyoxylate shunt were considered only in the study of Pgi mutant (Supporting Information Table S-I). The model for acetate consumption was composed of the TCA cycle, the anaplerotic pathway, the glyoxylate shunt, and part of the

gluconeogenic pathway (Supporting Information Table S-II). The same ^{13}C -MFA procedures as previously described were employed in this analysis.²⁴ It is important to note that, in this study, the mass isotopomer distributions of the intermediate metabolites were used, instead of the mass isotopomer distributions of the proteinogenic amino acids. The mass isotopomer distributions of F16P, DHAP, 3PG, PEP, PYR, Ru5P, R5P, S7P, and MAL were used for ^{13}C -MFA during the glucose consumption phase (39 independent data points). Likewise, the mass isotopomer distributions of MAL were used for ^{13}C -MFA during the acetate consumption phase. The mass isotopomer distributions of the measured compounds were corrected based on the method of van Winden et al.,²⁵ taking into account the natural isotope abundances of C, H, and O atoms. The fluxes for biomass synthesis were calculated from the *E. coli* biomass content.²⁶ The metabolic flux distributions were optimized by iteratively determining the mass isotopomer distributions computed from the assumed fluxes as the best fits to the measured mass isotopomer distributions of the metabolites. A genetic algorithm was combined with a sequential quadratic programming method to perform these optimizations.²⁷ The quality of the fit was confirmed by the χ^2 -test. The comparisons between simulated and experimental data of wild-type, Pyk mutant and Pgi mutant are given in Appendix Figure A1. All calculations were carried out using MATLAB R2006b with the Genetic Algorithm and Direct Search Toolbox 2.0.1 (Mathworks).

FBA

FBA is a constraint-based approach used to predict steady-state fluxes by applying mass balance constraints and objective function(s). It has been described in detail elsewhere.²⁸ Although the stoichiometric reaction model of FBA was almost the same as the model for ^{13}C -MFA, the mass balances of cofactors such as ATP, NADP, and NADPH were also considered in this analysis. Therefore, the electron transport chain reactions were added to the model (Supporting Information Table S-III). The P-to-O ratios were assumed to be 2.5 and 1.5 for NADH and FADH₂, respectively. We applied two different linear objective functions, specifically the maximization of biomass yield^{29,30} and the maximization of ATP production.³¹ In the case of the maximization of ATP production, the summation of the fluxes for Pgi, Pyk, SCS, Ack, and ATP synthase was maximized, and the specific growth rate was set to the experimentally determined value. Linear optimization was carried out using MATLAB R2006b with the Optimization Toolbox 3.0.3 (Mathworks).

Results and Discussion

The dynamics of the mass isotopomer distributions in continuous culture

To determine the different responses of mass isotopomer distributions, we conducted a continuous culture of wild-type strain BW25113 at a dilution rate of 0.5 h⁻¹. After starting ^{13}C -label, samples for the proteinogenic amino acids and for the intermediate metabolites were taken at the same time and the mass isotopomer distributions were measured. The time-courses of the mass isotopomer distributions of the proteinogenic amino acids and the intermediate metabolites are shown in Figures 1a,b, respectively. The lines in Figure 1a

were obtained by assuming the first-order washout kinetics,³² while the lines in Figure 1b were obtained through the measured concentrations of the intermediate metabolites with the steady-state fluxes.¹⁶

Figure 1a indicates that the responses of the mass isotopomers of all the proteinogenic amino acids were slow to converge to the isotopic steady-state, with convergence taking more than 5 hours from the start of the ^{13}C -labeling experiment. In contrast, Figure 1b indicates that the responses of the intermediate metabolites, such as 3PG, PYR, MAL, and PEP, were much faster and converged within minutes to the isotopic steady-state. The responses of the isotopomers for Ru5P and S7P were slightly slower in reaching the isotopic steady-state than the other isotopomers, a fact that may be due to the effect of the low fluxes in the PP pathway. Figure 1 indicates that the isotopomer distributions of intermediate metabolites response to flux changes much faster than that of proteinogenic amino acids.

Batch cultivations

Aerobic batch cultures of the wild-type strain and the Pyk and Pgi mutants were grown using glucose as a carbon source. Figure 2a shows the time-courses for cell growth and the extracellular concentrations of glucose and acetate, together with their corresponding specific rates in the wild-type batch culture. During the initial cell growth phase, glucose was consumed and acetate was produced. This growth phase lasted for 7 h, after which the cell growth rate rapidly decreased, in accordance with the depletion of glucose. The specific acetate production rate gradually decreased from 5 to 7 h. After the extracellular glucose was depleted, the cells began to consume acetate, and they continued to grow slowly from 8 to 9 h (late growth phase). Although the cell growth rate decreased during that time, the acetate consumption rate increased from 8 to 9 h, and the cells entered the stationary phase (a phase without cell growth) after the acetate was depleted.

Figure 2b shows the results of the Pyk and Pgi mutant cultures. The growth rate of the Pyk mutant was similar to that of the wild-type. By contrast, the growth rate of the Pgi mutant strain was much lower than that of the wild-type, displaying a nearly constant specific growth rate of about 0.2 h⁻¹ from 16 to 23 h.

Changes in mass isotopomer distributions of intermediate metabolites and proteinogenic amino acids during batch culture of the wild-type

Figure 3 shows the time-courses of the mass isotopomer distributions of the intermediate metabolites and the proteinogenic amino acids during the batch culture of wild-type *E. coli*. The mass isotopomer distributions of all proteinogenic amino acids were nearly constant throughout the cultivation, thus preventing us from estimating the flux changes during the batch culture. Conversely, the mass isotopomer distributions of the intermediate metabolites changed in the time-course, particularly during the late growth phase and the stationary phase. Specifically, after depletion of the glucose, the mass isotopomer distributions of the intermediate metabolites changed quickly as acetate was consumed. This change in the distributions implies drastic changes in the cell metabolism with the shift to acetate consumption. Together, our results imply that the metabolic fluxes were mostly

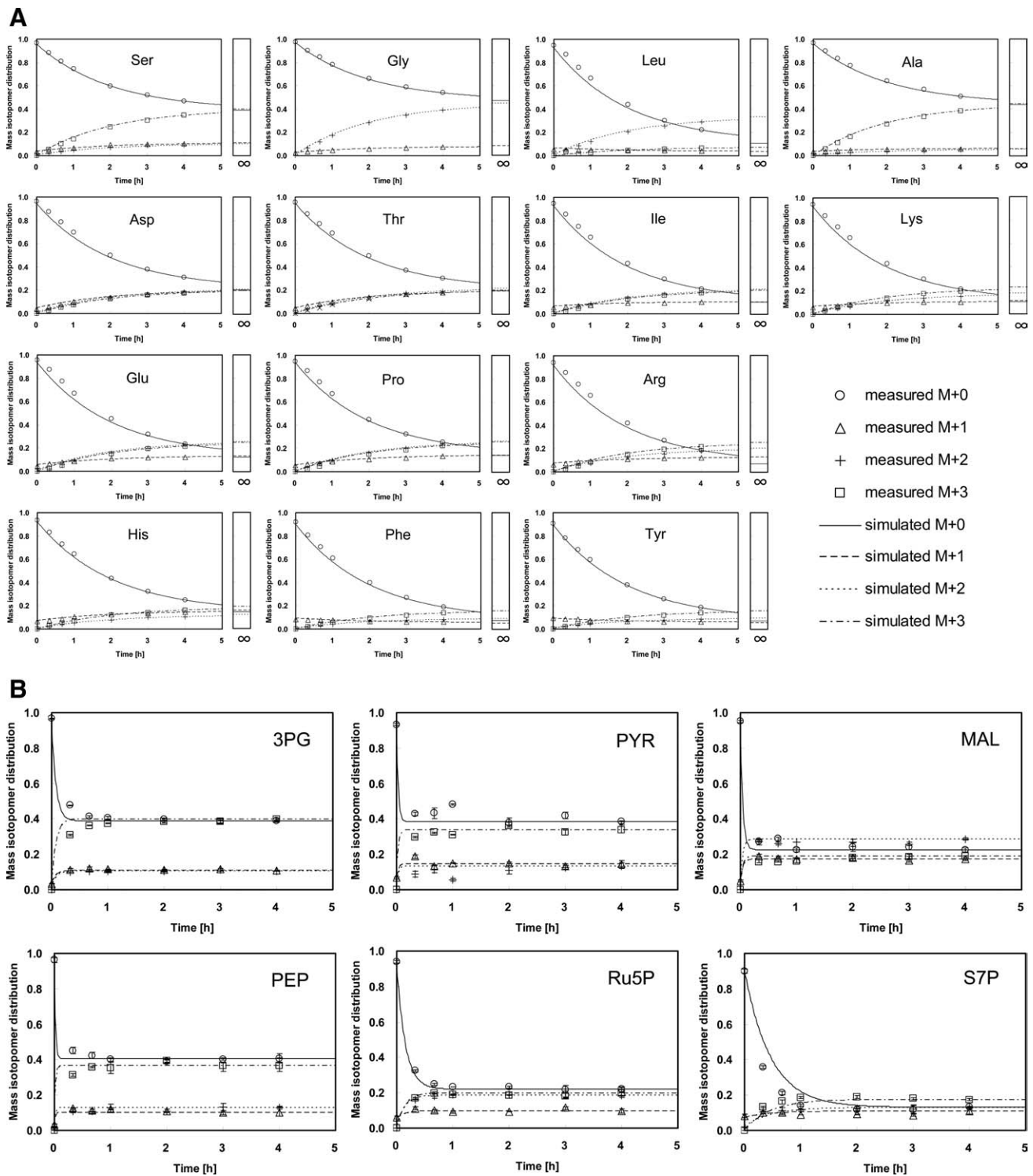


Figure 1. The differences between transients to reach isotopically steady-states for (a) proteinogenic amino acids and (b) intermediate metabolites.

All data are the averages of three measurements, and the error bars indicate the maximum and minimum values of the measurements. The concentrations \pm s indicate the standard deviations of the seven time point measurements during the ^{13}C -labeling experiment for 3PG, PYR, MAL, Ru5P, PEP, and S7P in the steady-state were 490 ± 123 , 122 ± 40 , 150 ± 88 , 150 ± 25 , 130 ± 23 , and $99 \pm 22 \mu\text{M}$, respectively.

constant during the cell growth phase but changed drastically in response to the change in carbon source from glucose to acetate. Note that the mass isotopomer distributions of the metabolites in the lower part of glycolysis and the TCA cycle, such as DHAP, 3PG, PEP, PYR, and MAL, changed during the late growth phase and returned to their original values after entry into the stationary phase.

Dynamic changes of the metabolite levels and fluxes during batch cultivation of wild-type

Metabolic fluxes were estimated using the mass isotopomer distributions of the intracellular metabolites measured by CE-TOFMS at 5, 6, 7, 8, 8.5, and 9 h. It was not easy to analyze at 4 h, since the cell concentration was low and the specific rates could not be accurately obtained. The

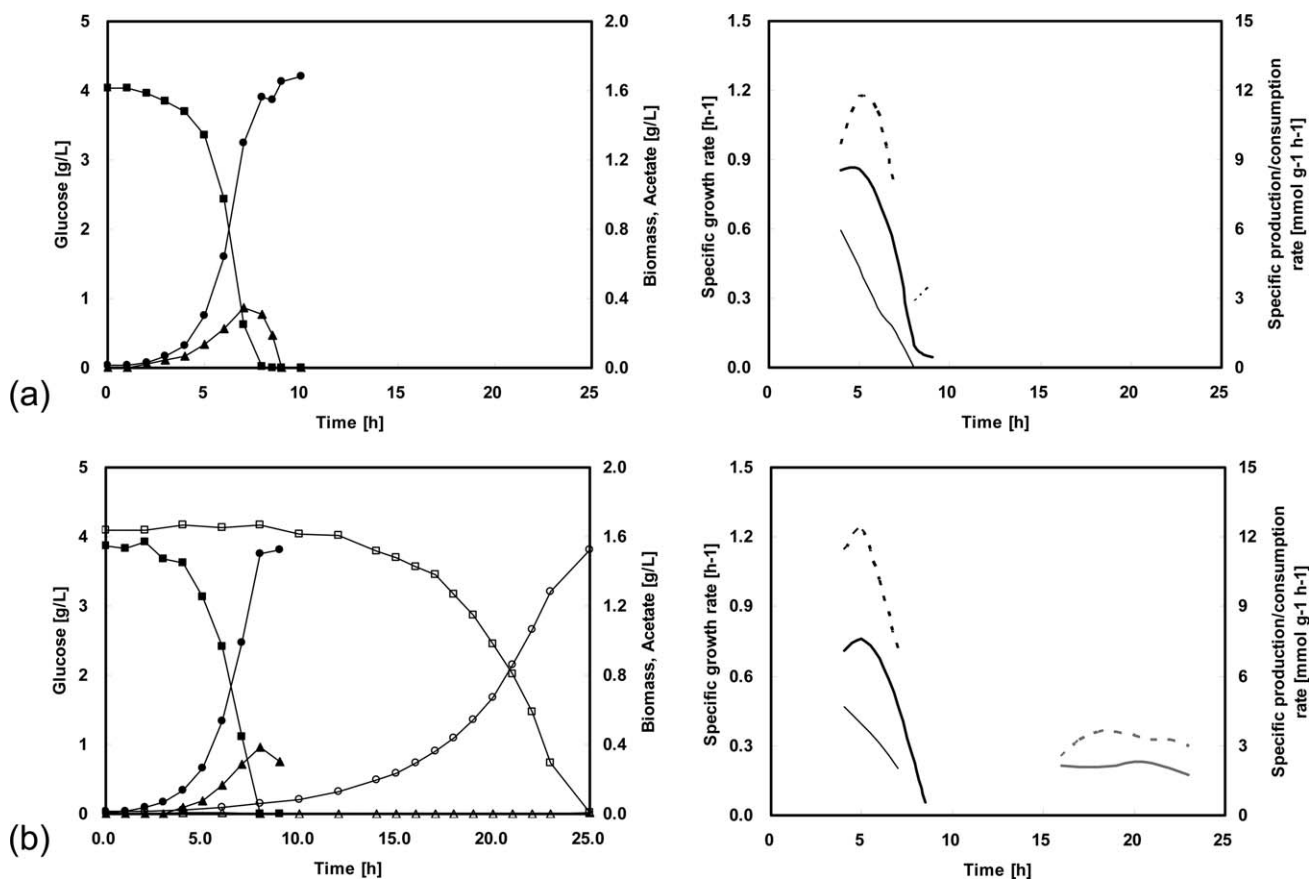


Figure 2. Aerobic batch cultivation of (a) wild-type and (b) Pyk and Pgi mutants.

Filled black circles, biomass of wild-type and Pyk mutants; filled black squares, glucose level in wild-type and Pyk mutants; filled black triangles, acetate level in wild-type and Pyk mutants; open circles, biomass of Pgi mutant strain; open squares, glucose level in Pgi mutant strain; open triangles, acetate level in Pgi mutant strain; bold line, specific growth rate of wild-type and Pyk mutant; bold broken line, specific glucose consumption rate of wild-type and Pyk mutant; thin line, specific acetate production rate of wild-type and Pyk mutant; thin broken line; specific acetate consumption rate of wild-type; gray bold line, specific growth rate of Pgi mutant; gray bold broken line, specific glucose consumption rate of Pgi mutant.

physiology at 4 h may be similar to that at 5 h. In the case at 10 h, acetate was depleted and the physiology may be complicated in this period, which is beyond the scope of the present article. When using glucose as the carbon source, the fluxes of the ED and the glyoxylate pathways were negligible in the wild-type strain.³³ Therefore, these reactions were not included in the model. Initially, the exchange fluxes of Pgi, Eno, Tk1, Tal, Tk2, MDH, and Ppc/Pck were considered. However, the χ^2 values for the determined fluxes in the batch culture were calculated as 870, 651, and 421 at 5, 6, and 7 h, respectively. These high χ^2 values were mainly come from the errors in F16P, DHAP, and S7P. To overcome this problem, we added the exchange fluxes of Fba, Tpi, Rpe, and Rpi into the model (13 degrees of freedom; 28 net reactions, 11 exchange coefficients, and two constraints as the acetate production rate and the growth rate). The resulting χ^2 values were improved to 168, 56, and 63 at 5, 6, and 7 h, respectively. These low χ^2 values ensured good agreement between the simulated and experimental data (Supporting Information Table S-VIII), indicating that the estimated fluxes were reliable. Figure 4a shows the estimated fluxes ($\text{mmol g}_{\text{DW}}^{-1} \text{h}^{-1}$) at 5, 6, and 7 h (from top to bottom), the period during which glucose was consumed as a carbon source. As can be seen in Figure 4a, the glycolysis flux changed little, whereas the TCA cycle flux increased from 5 to 6 h and decreased at 7 h. As we had previously observed that the acetate production rate decreased with respect to time (Fig. 2a), the increase of the TCA cycle flux

at 6 h may have been responsible for this decrease in the formation rate of acetate.³⁴

When using acetate as a carbon source, it has been known that the glyoxylate pathway becomes active, due to the activation of the *aceBAK* operon, which is caused by a decrease in FadR and IclR.^{35,36} For this reason, the glyoxylate pathway was included in the model for the late growth phase at 8, 8.5, and 9 h. Since the labeling pattern of MAL provides information on the flux ratio at the branch point between the glyoxylate pathway and the TCA cycle, the flux ratio was determined from the labeling pattern of the acetate in the medium and the mass isotopomer distribution of MAL. Since the concentrations of the intermediate metabolites in the glycolysis and PP pathways were low, the fluxes for these pathways were not included in the model of the late growth phase. Figure 4b shows the estimated metabolic fluxes at 8, 8.5, and 9 h, where the measured isotopomer distribution $[I_{00}, I_{01}, I_{10}, I_{11}]$ of acetate in the medium was $[0.667, 0.140, 0.003, 0.190]$. As can be seen in Figure 4b, the glyoxylate pathway flux was approximately constant at $1.2 \text{ mmol g}_{\text{DW}}^{-1} \text{h}^{-1}$ from 8 to 9 h. However, the ratio of the glyoxylate pathway flux to the TCA flux decreased during this time period. The glyoxylate pathway bypasses the two decarboxylation reactions in the TCA cycle in exchange for energy production. When the extracellular levels of acetate decreased, however, the TCA cycle was activated, suggesting that the cell was working to obtain energy for survival during the stationary phase.

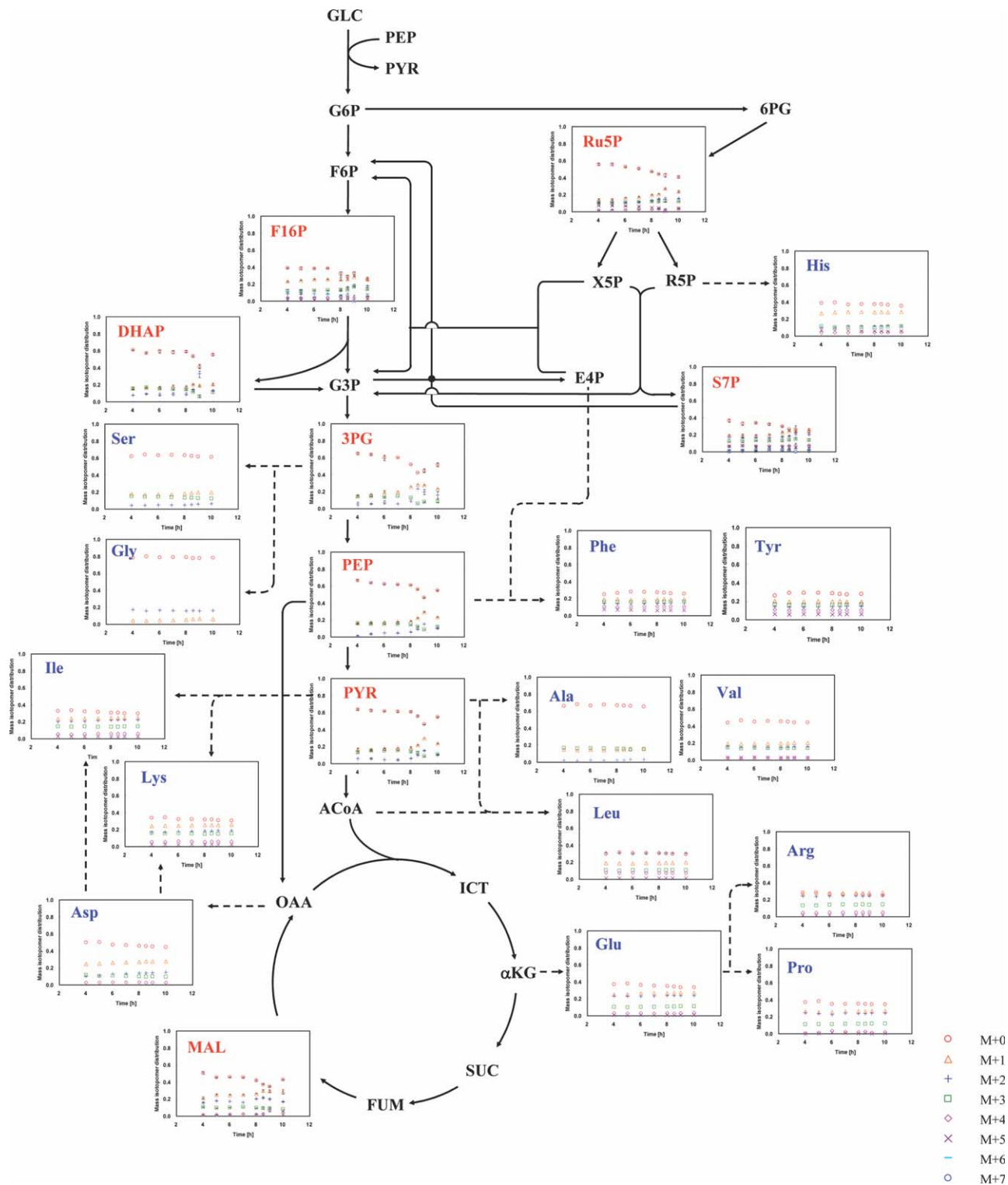


Figure 3. Time-series mass isotopomer distribution of intermediate metabolites and proteinogetic amino acids during batch culture.

Red, intermediate metabolite; blue, proteinogetic amino acid; dashed arrow, amino acid synthetic reactions. The reason for not using G6P was that the peaks of G6P and F6P could not be fully discriminated by CE. While the amounts of G6P were reliably determined because total amount of F6P was much smaller than G6P, some of isotopomer quantification might be affected by the corresponding isotopomer of F6P. Thus the mass isotopomer distribution of G6P was not used for the flux analyses.

Figure 5 shows the time-courses of the intermediate metabolite and free amino acid concentrations. Figure 5a indicates that the intermediate metabolite concentrations all remained low in the wild-type. Furthermore, the concentrations of metabolites such as G6P, F16P, DHAP, Ru5P, R5P, and S7P were maintained at relatively constant levels, whereas the levels of 3PG, PEP, and MAL increased about

threefold, and the level of PYR decreased from 5 to 7 h (Fig. 5a); the former metabolites belong to the upper part of the glycolysis and PP pathways. The changes in concentration of these metabolites may be related to the decrease in the Pyk flux and the increase in the Ppc and Mez fluxes. Specifically, the Ppc flux increased from 16 to 28%, and the fluxes of Pyk and PTS decreased from 100 to 83%.

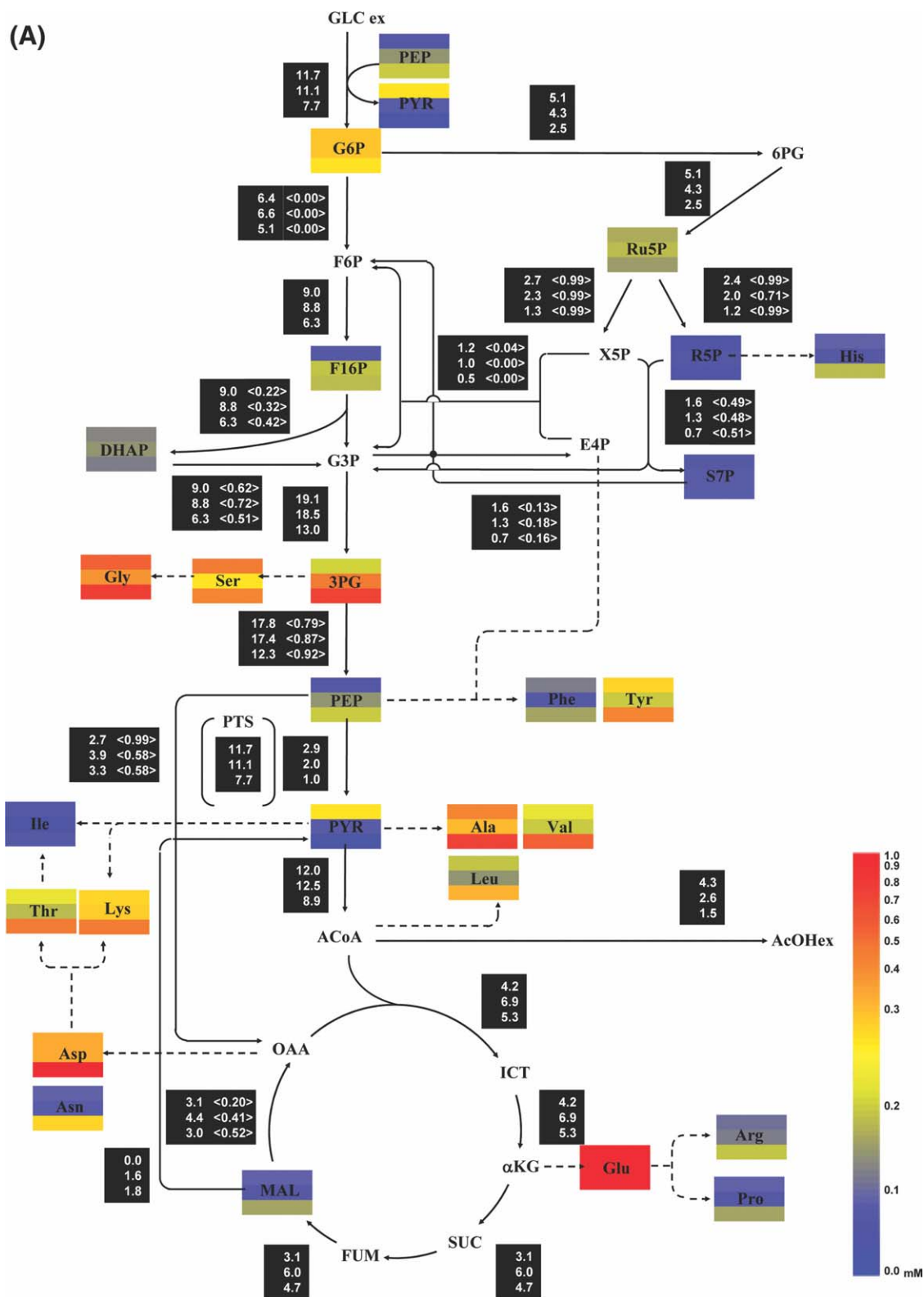


Figure 4. Metabolic flux distributions of wild-type *E. coli* (a) during the glucose consumption phase at 5 h (top), 6 h (middle), and 7 h (bottom), (b) during the acetate consumption phase at 8 h (top), 8.5 h (middle) and 9 h (bottom) in batch culture.

All fluxes are given as absolute values (mmol g⁻¹ h⁻¹), and the exchange coefficients are shown in angle brackets (< >). The relative flux values for the specific consumption rates are shown in Supporting Information Tables S-IV and S-V.

During the late growth phase, the concentrations of all metabolites were maintained at low levels, while the concentrations of many free amino acids, excluding His, Phe, and Tyr, significantly increased from 8.5 to 9 h when the gluconeogenic pathways were activated (Fig. 5). The low concen-

trations of His, Phe, and Tyr may have been due to low flux through gluconeogenesis. After the depletion of acetate, the free amino acid concentrations decreased rapidly. As previously discussed, the mass isotopomer distributions of the intermediate metabolites (DHAP, 3PG, PEP, PYR, and MAL),

(B)

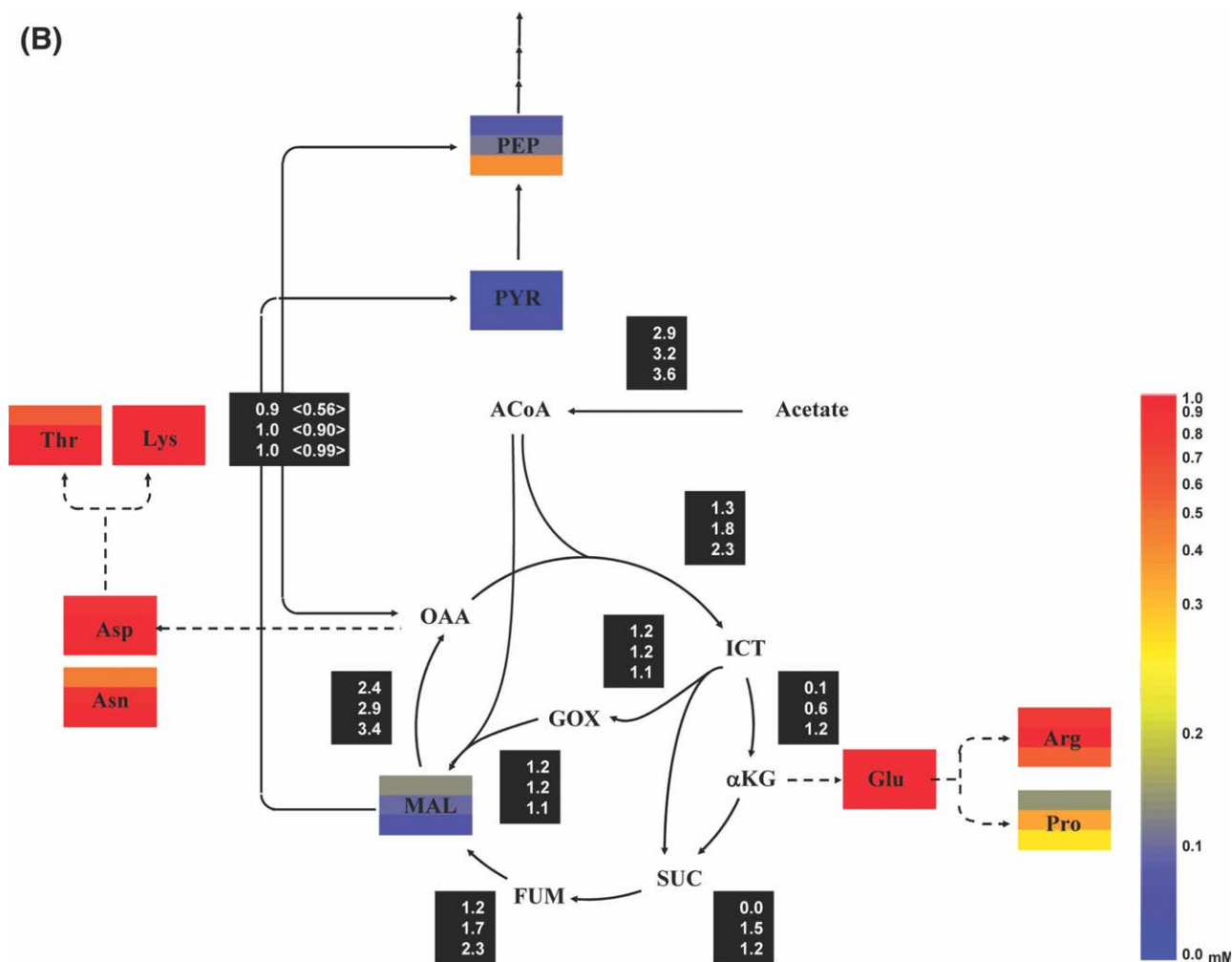


Figure 4. Continued

which changed during the late growth phase, returned to their original values during stationary phase (Fig. 3). These changes might be the result of the degradation of proteins into free amino acids by cellular autophagy to use those amino acids for energy or cell maintenance.

Fluxes and metabolite levels in the *Pyk* mutant strain during batch cultivation

Figure 6 shows the changes in metabolic flux in the *Pyk* mutant strain during the batch culture at 5, 6, and 7 h. *Pyk* catalyzes the conversion of PEP and ADP to PYR and ATP in the final step of glycolysis. Although the *Pyk* reaction was completely shut down in the *pykF* and *pykA* genes knockout mutant, PEP can still be converted to PYR through PTS. In addition, the ED and glyoxylate pathways are negligible in the *Pyk* mutant.¹⁸ Therefore, those pathways were not included in the model. Furthermore, the same exchange reactions as wild-type were considered (12 degrees of freedom; 28 net reactions, 11 exchange coefficients, and three constraints as the deletion of *Pyk* reaction, the acetate production rate, and the growth rate).

Figure 5a illustrates the accumulation of metabolites, such as G6P, F16P, DHAP, Ru5P, R5P, and S7P, that peaked at 5 to 6 h. Since the concentrations of the metabolites closer to PEP tended to be high, the accumulation of these metabolites is likely due to dumping caused by the accumulation of PEP.

Concentrations of these metabolites stopped increasing and began decreasing after 6 h, while the same shift for the PEP and 3PG concentrations was delayed by from half an hour to 1 hour. This may have been caused by the reduced flux from the previous steps in the upper part of the glycolysis pathway. In particular, the accumulation of PEP may have resulted in allosteric inhibition of Pfk, a rate limiting enzyme in the upper part of glycolysis.³⁷ Note that G6P accumulated slightly at 6 h due to Pfk inhibition by PEP, which may have resulted in a lower uptake rate of glucose.

Figure 5a also shows that the accumulation of PEP resulted in the higher Ppc flux, which in turn increased the concentrations of OAA and MAL, particularly from 5 to 6 h. The increased concentration of MAL caused the Mez flux to increase. Thus, the reduced amount of PYR backed up, and the ratio of PYR provided via Mez (from 23 to 26%) was larger in the mutant than the ratio seen in the wild-type strain (from 0 to 11%). Furthermore, the exchange coefficient of MDH was significantly higher (>0.99) from 5 to 7 h. After 6 h, the concentration of MAL decreased, possibly due to the reduced flux through the Ppc pathway. Since the concentration of ACoA changed little from 6 to 7 h, the concentration of ACoA, which is an important activator of Ppc, may have decreased during this period as well.³⁸

Despite the dramatic changes in the concentrations of many intermediate metabolites, the branch ratio between glycolysis and the PP pathway in the mutant strain was similar

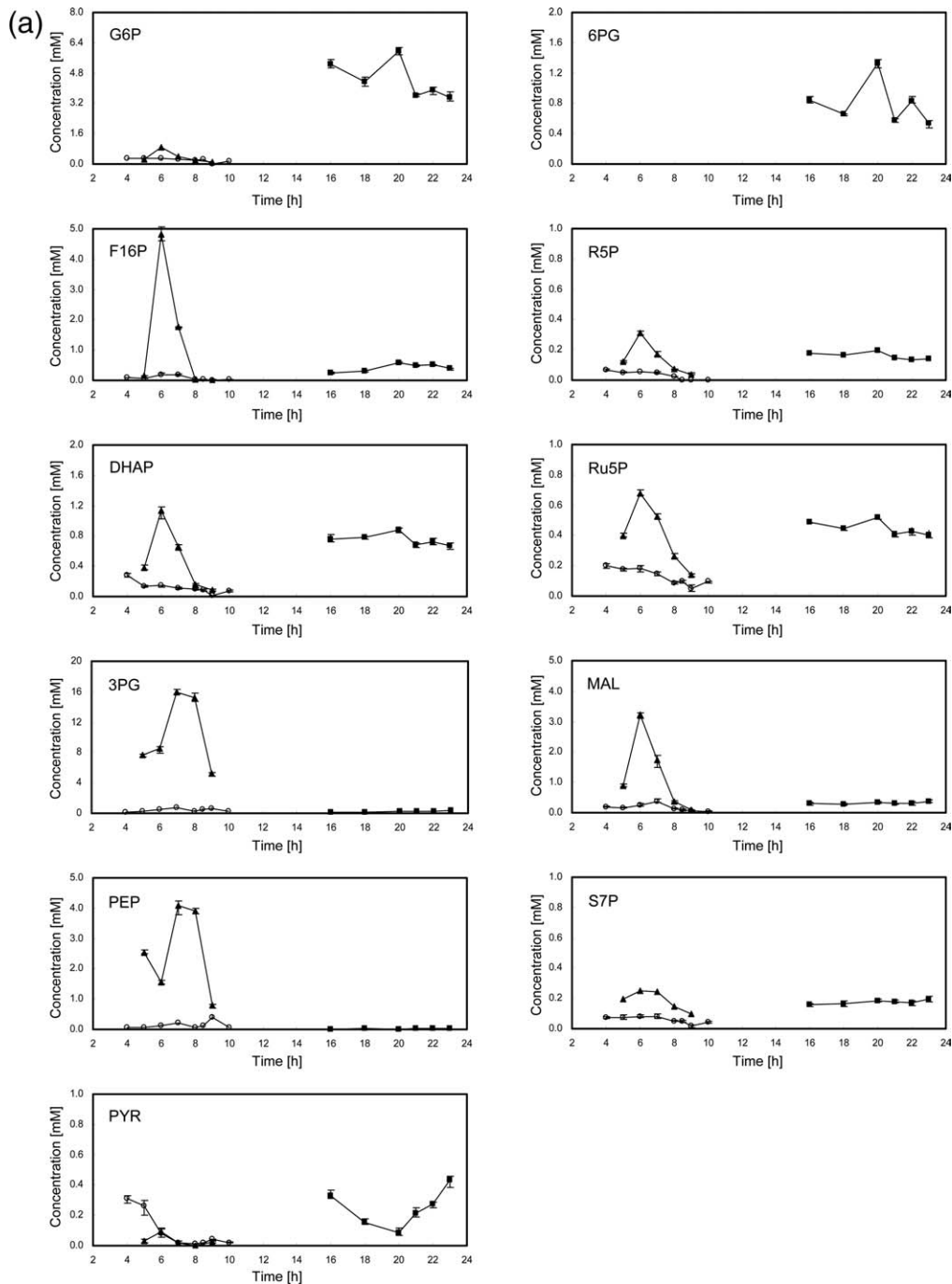


Figure 5. Time-series concentrations of (a) the intermediate metabolites and (b) the free amino acids in the batch culture of wild-type *E. coli* and in the Pyk and Pgi mutant strains.

Open circles, the concentration in wild-type; filled black triangles, the concentration in the Pyk mutant strain; filled black squares, the concentration in the Pgi mutant strain. Note that some free amino acid concentrations may be overestimated due to the effect of leaked amino acids from the cut-off filter used for preparation of the CE-TOFMS measurement.

to that of the wild-type at 5 h. The glycolysis flux decreased, but the PP pathway flux changed little from 5 to 6 h, the period when most of the intermediate metabolites accumulated significantly. At 6 h, G6P concentration rose slightly (0.85 mM), possibly due to Pfk inhibition, as previously discussed. As a result, the accumulated G6P suppressed the glucose uptake rate and activated the G6PDH flux in the oxidative PP pathway.

It is important to note that the exchange coefficients of Pgi, Fba, and Tpi in the Pyk mutant were higher than the coefficients in the wild-type strain. For example, the

exchange coefficient of Pgi was 0.00 from 5 to 7 h in the wild-type, while the same coefficient was substantially higher, from 0.30 to 0.60, in the Pyk mutant.

Despite the changes in the intermediate metabolite concentrations, all the measured free amino acid concentrations changed little from 5 to 7 h in the Pyk mutant. Moreover, the concentrations of free amino acids in the mutant strain were similar to those in the wild-type (Fig. 5b). This result coincides with the similar growth rates between the mutant and wild-type strains, and it suggests that amino acid synthesis is very robust.

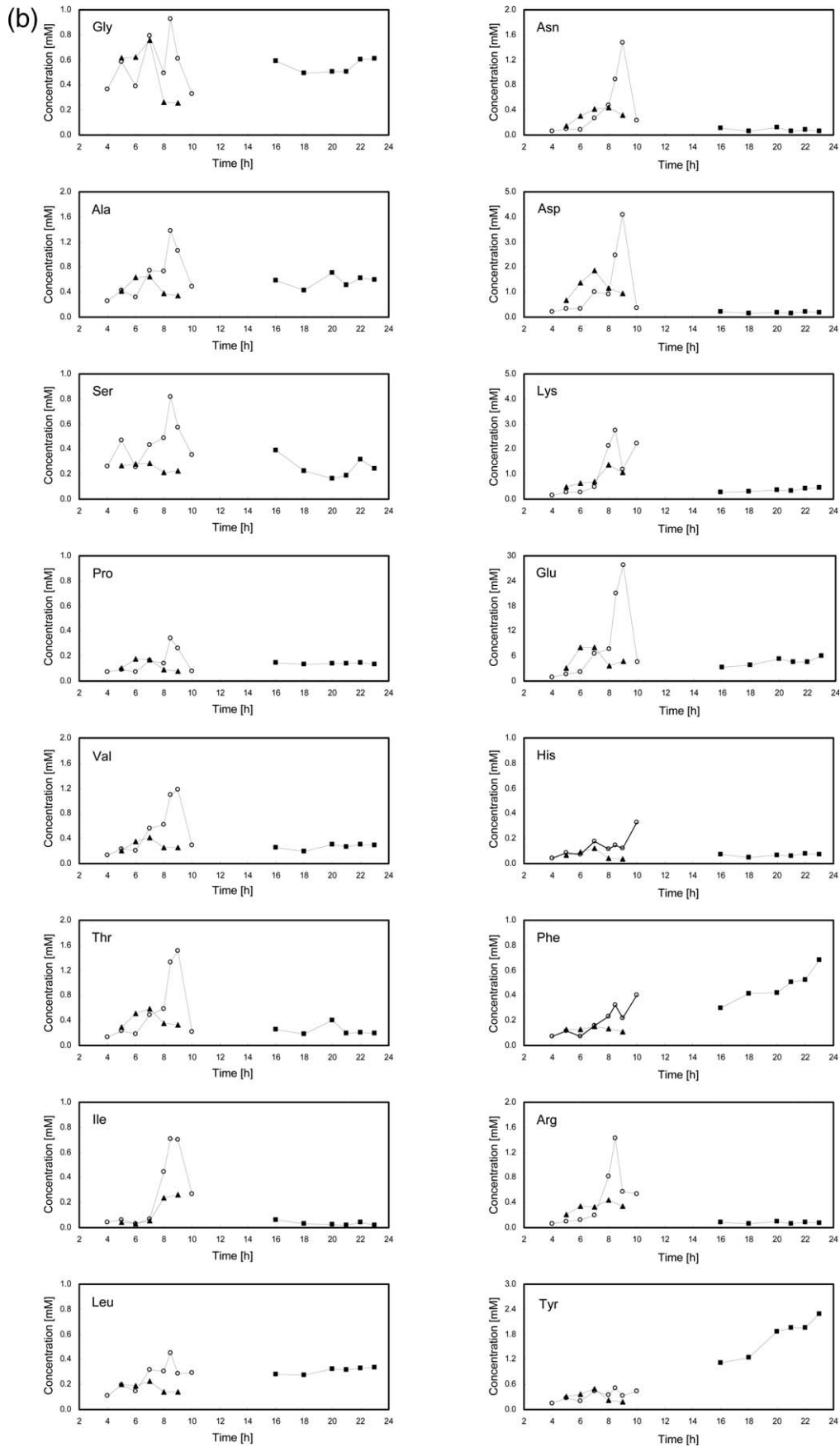


Figure 5. Continued

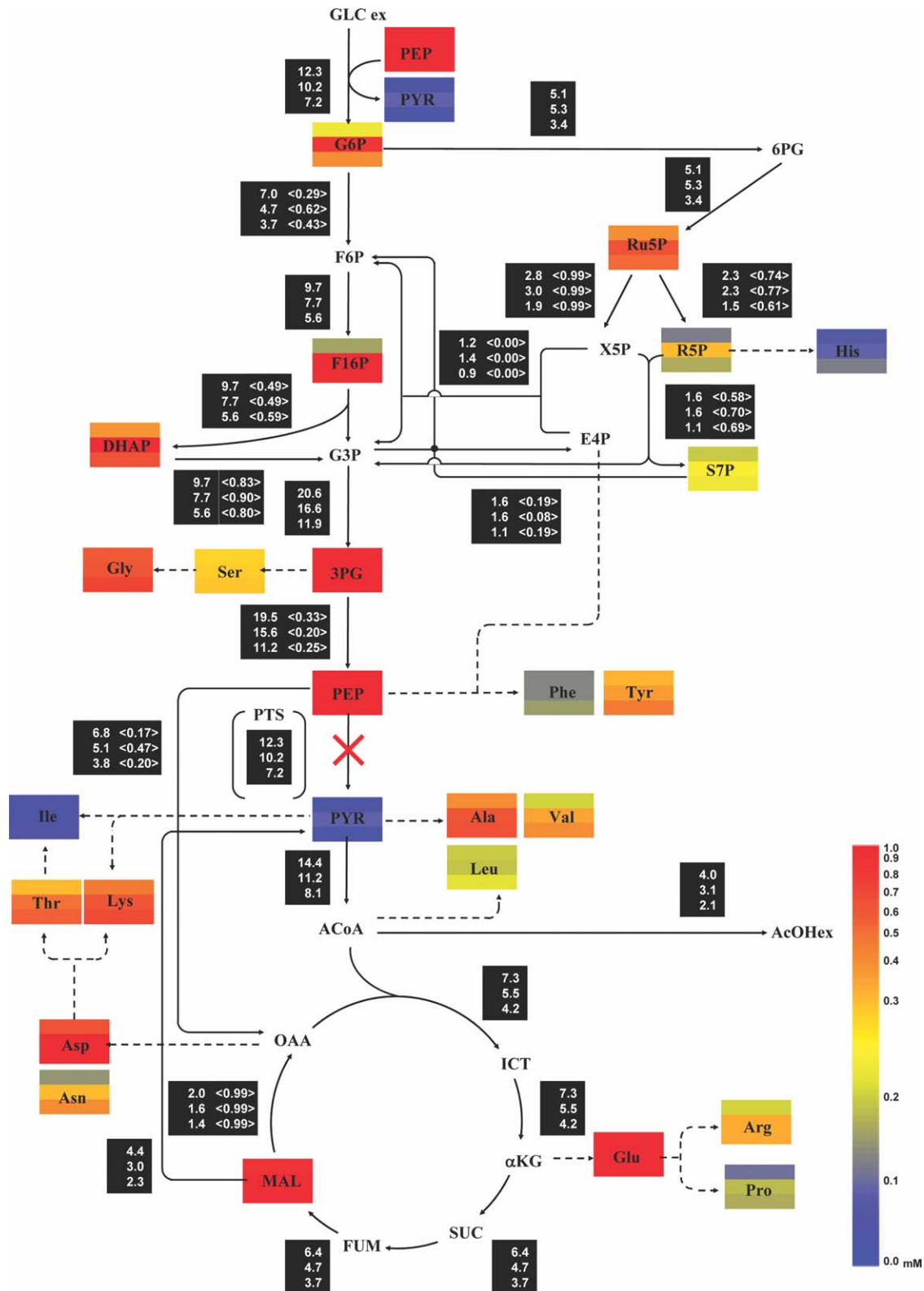


Figure 6. Metabolic flux distributions of the Pyk mutant strain at 5 h (top), 6 h (middle), and 7 h (bottom) in batch culture.

The χ^2 values were 49, 92, and 51 for the batch culture at 5, 6, and 7 h, respectively. The relative flux values of the specific glucose consumption rates are shown in Supporting Information Table S-VI. The comparison between simulated data and experimental data is shown in Supporting Information Table S-IX.

Flux and metabolite levels in the Pgi mutant strain during batch cultivation

Figure 7 shows the change in the metabolic fluxes at 16, 21, and 23 h in the Pgi mutant strain during the cell growth

phase. The same exchange reactions as wild-type except Pgi were considered in the model (13 degrees of freedom; 30 net reactions, 10 exchange coefficients, and two constraints as the deletion of Pgi reaction, and the growth rate). Pgi

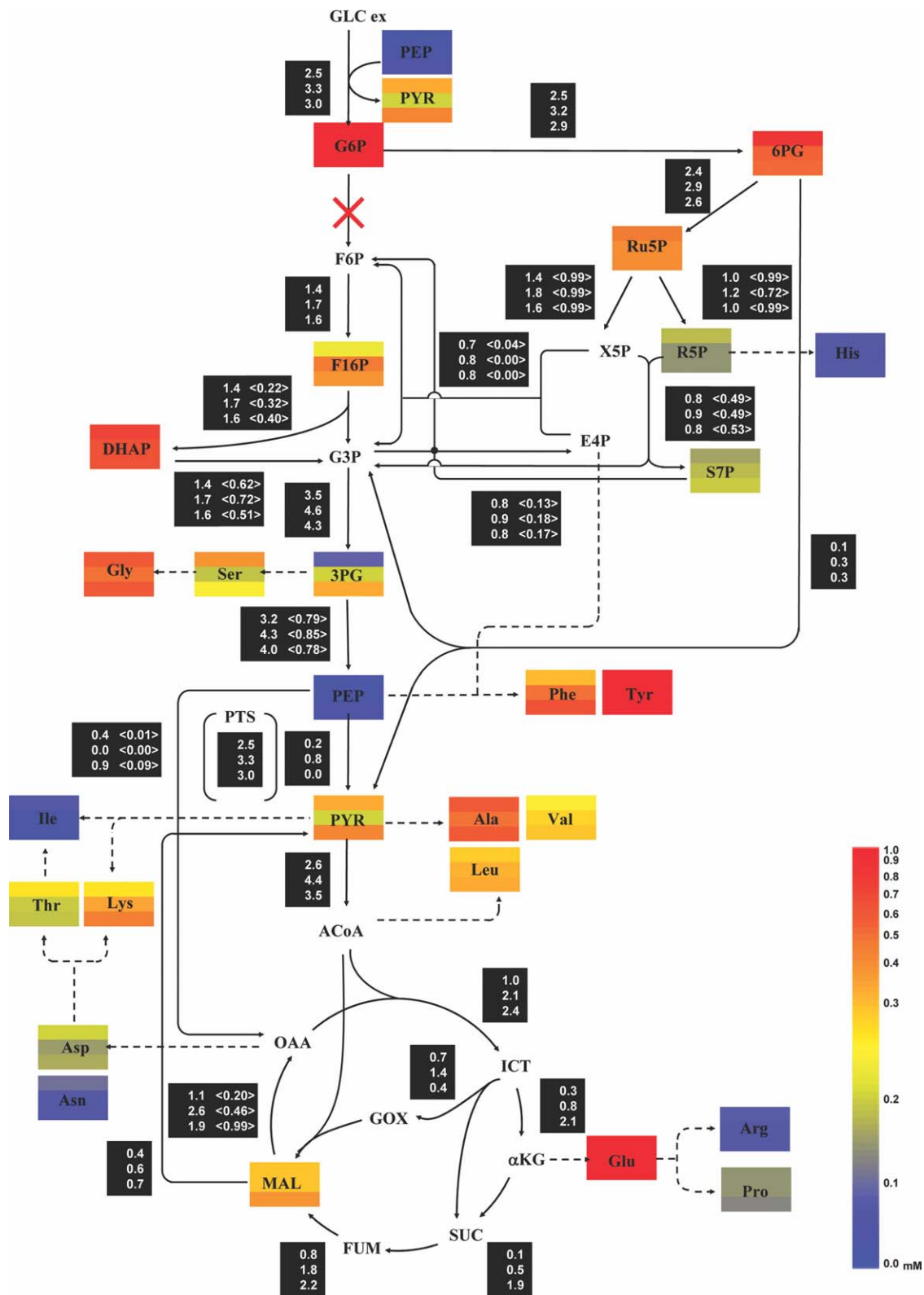


Figure 7. Metabolic flux distributions of the Pgi mutant strain at 16 h (top), 21 h (middle), and 23 h (bottom) in batch culture.

The χ^2 values were 197, 197, and 299 for the batch culture at 16, 21, and 23 h, respectively. The relative flux values of the specific glucose consumption rates are shown in Supporting Information Table S-VII. The comparison between simulated data and experimental data is shown in Supporting Information Table S-X.

catalyzes the conversion of G6P to F6P during the initial step of glycolysis. In the Pgi mutant, glucose uptake occurs only through the PP pathway. The specific growth rate of the Pgi mutant remained constant at $\sim 0.2 \text{ h}^{-1}$ from 16 to 23 h (Fig. 2b), and the overall fluxes and the intermediate metab-

olite concentrations changed little over time (Fig. 7). Furthermore, these fluxes values, as well as the intermediate metabolite concentrations (except for the concentrations of G6P and 6PG), were similar to those in the continuous culture at the 0.2 h^{-1} dilution rate.³⁹ Since G6P was most

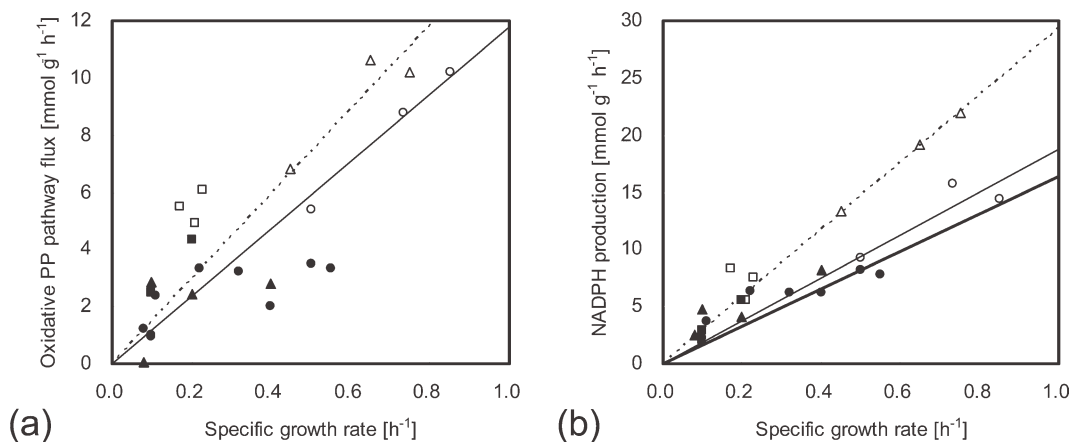


Figure 8. Comparison between the specific growth rates and (a) the oxidative PP pathway flux and (b) NADPH production in both the continuous cultures and the batch culture.

Open circle, the flux of wild-type in the continuous cultures; closed circle, the flux of wild-type in the batch culture; open triangle, the flux of the Pyk mutant strain in the continuous cultures; closed triangle, the flux of the Pyk mutant strain in the batch culture; open square, the flux of the Pgi mutant strain in the continuous cultures; closed square, the flux of the Pgi mutant strain in the batch culture; solid line, the linear approximation of the flux of the wild-type strain in the batch culture; dashed line, the linear approximation of the flux of the Pyk mutant strain in the batch culture; bold line, the specific amount of NADPH required, depending on the cell growth rate.

prominently accumulated, G6PDH reaction, which consumes most of G6P in this mutant, could be considered to be the rate-limiting step for growth. Although net flux of G6PDH was lower than wild-type or Pyk mutant, expected higher NADPH/NADP⁺ ratio could result in the lower maximum flux of this enzyme in Pgi mutant. The higher NADPH/NADP⁺ ratio was expected because of the higher rate of NADPH production/growth (see below), and had been confirmed at the exponential growth phase in batch culture.⁴⁰

The blockage of the Pgi reaction in this mutant strain resulted in low levels of accumulation of the intermediate metabolites in the later steps of glycolysis, such as 3PG and PEP, from 16 to 23 h. In particular, the concentration of PEP was significantly lower than in the wild-type (<0.04 mM, compared with 0.20 mM in the wild-type) because PEP is consumed not only by Pyk but also by PTS. The low concentration of PEP resulted in lower fluxes of Pyk and Ppc as compared to the wild-type. Lower fluxes through Ppc may have caused the OAA concentration to decrease. Furthermore, although the concentrations of many amino acids were maintained at similar levels to wild-type, the concentrations of amino acids such as Asp and Asn were lower in the mutant than in the wild-type (Fig. 5b). This may be due to the lower flux of the Ppc reaction. By contrast, the concentrations of the aromatic amino acids Phe and Tyr were clearly higher in the mutant than in the wild-type. Furthermore, the levels of these two amino acids increased over time in the mutant strain (Fig. 5b). Since Phe and Tyr are synthesized from two moles of PEP, one mole of E4P, and one mole of Glu via the shikimate pathway, the accumulation of Phe and Tyr in the Pgi mutant may be related to the activation of the PP pathway. Although the accumulation of E4P was not confirmed by measurement in the Pgi mutant, high levels of shikimate were detected in the Pgi mutant, indicating the activation of the shikimate pathway, whereas it was not detected in the wild-type strain.

Relationship between growth rate and metabolic fluxes in batch and continuous cultures

We have shown that the changes in flux during batch cultures of Pyk and Pgi mutants could be estimated over time

based on the mass isotopomer distributions of intermediate metabolites measured by CE-TOFMS. In the batch culture of Pyk mutant, PEP and other glycolysis intermediate concentrations were much higher than those in the continuous culture, and changed with respect to time. By the information on the metabolite concentrations and the ¹³C-metabolic fluxes, we found that the glycolysis was affected by not only the feedback inhibition by PEP but also the dumping of glycolysis intermediates in the batch culture. In the Pgi mutant, the flux distributions as well as intermediate metabolite concentrations except G6P were similar between batch and continuous cultures at the same growth rate, where it was considered that G6PDH reaction was the limiting step for this mutant.

Once the changes in flux have been estimated, further analyses can be performed. For example, let us consider whether NADPH production is dependent on the growth rate. Figure 8a shows the correlation between the specific growth rate and the fluxes of the oxidative PP pathways (G6PDH and 6PGDH), using the fluxes obtained in the present study as well as data previously obtained from continuous culture.^{16–18,24,39,41,42} Cell growth requires a specific amount of NADPH that depends on the cell growth rate. NADPH is mainly produced by the oxidative PP pathway and the ICDH of the TCA cycle. In batch cultures of wild-type *E. coli*, the PP pathway flux increased in proportion to the specific growth rate. Since the concentration of G6P did not change substantially, the increase in these fluxes is likely due to the increase in the enzyme activity of G6PDH⁴³ or the decrease in the NADPH/NADP⁺ ratio. Conversely, in continuous cultures with dilution rates from 0.09 to 0.55 h⁻¹, the oxidative PP pathway flux increased less than in the batch cultures (~4 mmol g⁻¹ h⁻¹), even as the specific growth rates increased in accordance with the dilution rate. This difference may be caused by the low glucose concentration (less than 0.001 g/L) in the continuous culture, as G6PDH activity is induced by glucose.⁴⁴ Thus, the PP pathway flux was limited to ~4 mmol g⁻¹ h⁻¹ in the continuous culture. The flux of ICDH increased in proportion to the specific growth rate in the continuous culture, suggesting that the cells utilized ICDH instead of the PP pathway for production of NADPH. Figure 8a indicates that the relationship

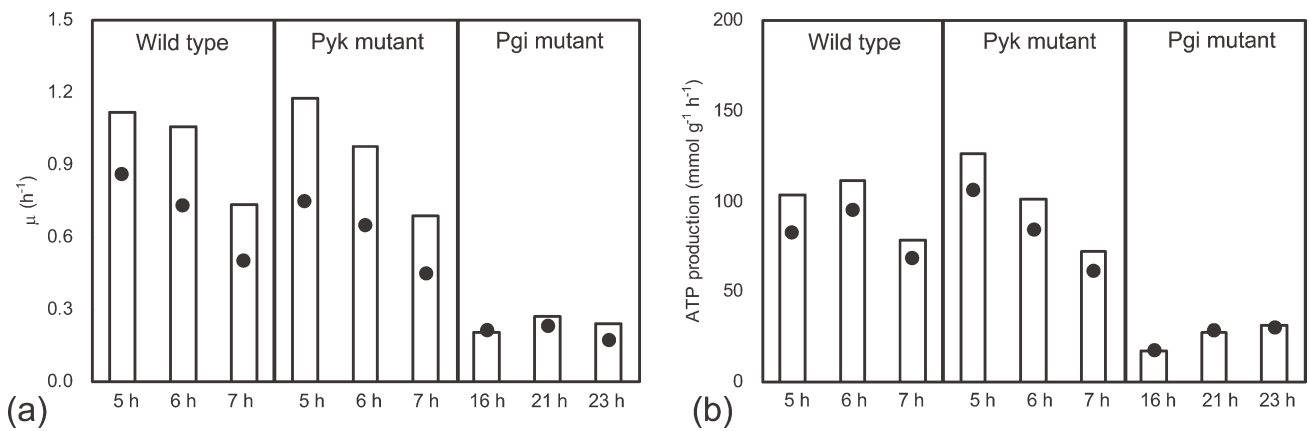


Figure 9. The maximum and measured growth rates (a) and ATP production rates (b) in the batch cultures of wild-type *E. coli* and in the Pyk and Pgi mutants.

Open bars, the maximized growth rates and ATP production rates predicted by FBA; filled circle, experimental growth rates and estimated ATP production rates determined by ^{13}C -MFA.

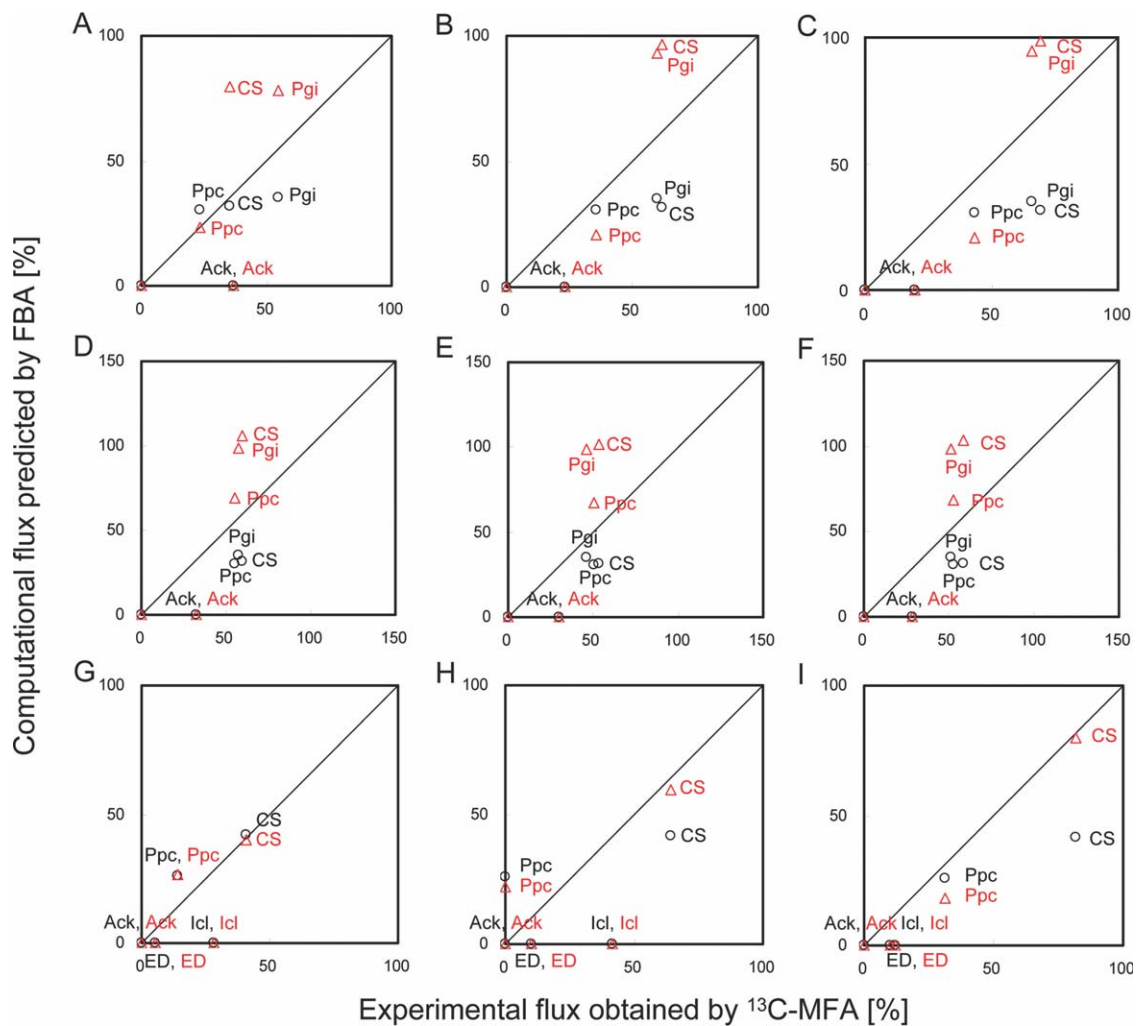


Figure 10. Comparisons of individual fluxes between ^{13}C -MFA and FBA.

A to C show the comparisons at 5, 6, and 7 h in wild-type; D to F show the comparisons at 5, 6, and 7 h in the Pyk mutant strain; G to I show the comparisons at 16, 21, and 23 h in the Pgi mutant strain. Black open circle, the flux predicted by FBA with maximization of biomass yield; red open triangle, the flux predicted by FBA with maximization of ATP production. Fluxes are values given relative to the specific glucose consumption rate.

between the specific growth rate and the flux of the oxidative PP pathway in the wild-type cultures was similar to the relationship observed in the Pyk mutant strain. The correlations

between the specific growth rate and the total NADPH production rate are shown in Figure 8b. The line in Figure 8b represents the specific amount of NADPH required for cell

growth. It is worth noting that although the required amount of NADPH was produced in both the batch and continuous cultures of the wild-type strain, excess NADPH was produced by the Pyk and Pgi mutants in batch culture. It has been reported that the overproduced NADPH in the Pgi mutant is converted into NADH by the transhydrogenase.⁴⁵ The Pyk mutant may also convert excess NADPH into NADH using transhydrogenase.⁴¹

Evaluation of ¹³C-MFA by FBA

From the systems biology viewpoint, metabolic fluxes may be predicted by optimizing a vector-valued objective function consisting of objectives such as energy production, biomass production, enzyme usage, and redox balance.³¹ The weight for each objective function may change with respect to time. Once the metabolic fluxes are determined through the use of ¹³C-MFA, each objective function can be evaluated. Since FBA is a computational method used to predict the flux distribution by optimizing a given objective function,²⁸ we also performed FBA using two different objective functions, specifically biomass yield^{29,30} and ATP production.³¹

Figure 9 shows the comparison of the maximum growth rates (Fig. 9a) and the maximum ATP production rates (Fig. 9b) determined by ¹³C-MFA with those predicted by FBA. The experimentally measured growth rates and the ATP production rates estimated by ¹³C-MFA were smaller than those estimated by FBA in the wild-type and the Pyk mutant strains. However, the estimated and measured values were similar in the Pgi mutant. The disagreement between the estimated and measured values for the wild-type and the Pyk mutant strains implies that each objective function is not fully optimized, but may be utilized to some extent. The good agreement in the case of the Pgi mutant strain indicates that both objective functions were optimized for the Pgi mutant, in which ATP production seems to be more critical. Figure 10 shows the comparisons between individual fluxes obtained by ¹³C-MFA and FBA. Most of the fluxes obtained by ¹³C-MFA were located between those obtained by FBA using maximization of biomass yield and those obtained using maximization of ATP production in both the wild-type and Pyk mutant strains. For example, the Pgi flux estimated by FBA was larger than the value determined by ¹³C-MFA in the case of maximum ATP production. This may be due to the fact that the PP pathway does not contribute to ATP production, and thus the flux at G6P tended towards glycolysis in the FBA. By contrast, as the PP pathway becomes important for cell synthesis, the flux toward the PP pathway at G6P tends to be larger when using cell yield as an objective function. Since the predicted growth rates were larger than the experimental values, the Pgi fluxes were smaller than those estimated by ¹³C-MFA in the case of maximizing biomass yield.

A closer examination of Figures 10A–C suggests that the cell gave higher priority to biomass production than to ATP production at 5 h, while the priority of biomass production declined gradually from 5 to 7 h, indicating physiological changes from mid-log phase to end-log phase with glucose as a carbon source.⁴⁶ Figures 10D–F indicates that the Pyk mutant consistently gave high priority to biomass production from 5 to 7 h. Note that the acetate formations predicted by FBA using both functions were zero for the wild-type and the Pyk mutant, and they are different from those obtained

by ¹³C-experimental fluxes (Figures 10A–F). Although the acetate formation is associated with ATP production, more ATP can be produced in the TCA cycle, and thus the optimized flux at Pta-Ack pathway became zero. The acetate formation may be considered to be a result of the overflow metabolism, and thus this could not be addressed properly by FBA. Furthermore, Figures 10G–I indicates that FBA cannot predict the glyoxylate pathway flux for the Pgi mutant strain, because this pathway is a part of the anaplerotic pathway and does not contribute to ATP production.

In conclusion, the primary objective of this study was to investigate the cellular regulatory mechanisms of *E. coli* grown in batch culture based on the dynamics of both metabolic fluxes and intracellular metabolite concentrations. The integration of the fluxes estimated by ¹³C-MFA and metabolite concentrations provides a better understanding of how cells adjust their metabolism in response to environmental changes and/or genetic perturbations in batch cultures over time. Furthermore, it was shown that the objective function for biosynthesis became less important as time proceeds in the wild-type, while it remained important in the Pyk mutant. Furthermore, it was shown that ATP production was the primary objective function in the Pgi mutant.

Acknowledgments

The authors thank Yuji Kakazu and Akiyoshi Hirayama for informative discussions and technical advice. This research was supported by a Grant-in-Aid for JSPS Fellows (20-4722). Also supported by a CREST, JST (Development of Modeling/Simulation Environment for Systems Biology); the G-COE Program (Center for Human Metabolomics Systems Biology); the MEXT, Grant-in-Aid for Scientific Research on Priority Areas; and the Research fund provided by Yamagata Prefecture and Tsuruoka City.

Literature Cited

1. Wiechert W. ¹³C metabolic flux analysis. *Metab Eng.* 2001;3:195–206.
2. Shimizu K. Metabolic flux analysis based on ¹³C-labeling experiments and integration of the information with gene and protein expression patterns. *Adv Biochem Eng Biotechnol.* 2004;91:1–49.
3. Wittmann C. Fluxome analysis using GC-MS. *Microb Cell Fact.* 2007;6:6.
4. Wiechert W, Nöh K. From stationary to instationary metabolic flux analysis. *Adv Biochem Eng Biotechnol.* 2005;92:145–172.
5. Gaden EL. Fermentation process kinetics. *J Biochem Microbiological Technol Eng.* 1959;1:413–429.
6. Antoniewicz MR, Kraynie DF, Laffend LA, Gonzalez-Lergier J, Kelleher JK, Stephanopoulos G. Metabolic flux analysis in a nonstationary system: fed-batch fermentation of a high yielding strain of *E. coli* producing 1,3-propanediol. *Metab Eng.* 2007;9:277–292.
7. Iwatani S, Van Dien S, Shimbo K, Kubota K, Kageyama N, Iwahata D, Miyano H, Hirayama K, Usuda Y, Shimizu K, Matsui K. Determination of metabolic flux changes during fed-batch cultivation from measurements of intracellular amino acids by LC-MS/MS. *J Biotechnol.* 2007;128:93–111.
8. Nöh K, Gronke K, Luo B, Takors R, Oldiges M, Wiechert W. Metabolic flux analysis at ultra short time scale: isotopically non-stationary (¹³C) labeling experiments. *J Biotechnol.* 2007;129:249–267.
9. Schaub J, Mauch K, Reuss M. Metabolic flux analysis in *Escherichia coli* by integrating isotopic dynamic and isotopic stationary ¹³C labeling data. *Biotechnol Bioeng.* 2008;99:1170–1185.
10. Maier K, Hofmann U, Reuss M, Mauch K. Identification of metabolic fluxes in hepatic cells from transient ¹³C-labeling

- experiments: Part II. Flux estimation. *Biotechnol Bioeng.* 2008; 100:355–370.
11. Zhao Z, Kuijvenhoven K, Ras C, Van Gulik WM, Heijnen JJ, Verheijen PJ, Van Winden WA. Isotopic non-stationary ^{13}C gluconate tracer method for accurate determination of the pentose phosphate pathway split-ratio in *Penicillium chrysogenum*. *Metab Eng.* 2008;10:178–186.
 12. Young JD, Walther JL, Antoniewicz MR, Yoo H, Stephanopoulos G. An elementary metabolite unit (EMU) based method of isotopically nonstationary flux analysis. *Biotechnol Bioeng.* 2008;99:686–699.
 13. Costenoble R, Muller D, Barl T, Van Gulik WM, Van Winden WA, Reuss M, Heijnen JJ. ^{13}C -Labeled metabolic flux analysis of a fed-batch culture of elutriated *Saccharomyces cerevisiae*. *FEMS Yeast Res.* 2007;7:511–526.
 14. Soga T, Baran R, Suematsu M, Ueno Y, Ikeda S, Sakurakawa T, Kakazu Y, Ishikawa T, Robert M, Nishioka T, Tomita M. Differential metabolomics reveals ophthalmic acid as an oxidative stress biomarker indicating hepatic glutathione consumption. *J Biol Chem.* 2006;281:16768–16776.
 15. Soga T, Ohashi Y, Ueno Y, Naraoka H, Tomita M, Nishioka T. Quantitative metabolome analysis using capillary electrophoresis mass spectrometry. *J Proteome Res.* 2003;2:488–494.
 16. Toya Y, Ishii N, Hirasawa T, Naba M, Hirai K, Sugawara K, Igarashi S, Shimizu K, Tomita M, Soga T. Direct measurement of isotopomer of intracellular metabolites using capillary electrophoresis time-of-flight mass spectrometry for efficient metabolic flux analysis. *J Chromatogr A.* 2007;1159:134–141.
 17. Hua Q, Yang C, Baba T, Mori H, Shimizu K. Responses of the central metabolism in *Escherichia coli* to phosphoglucose isomerase and glucose-6-phosphate dehydrogenase knockouts. *J Bacteriol.* 2003;185:7053–7067.
 18. Al Zaid Siddiquee K, Arauzo-Bravo MJ, Shimizu K. Metabolic flux analysis of *pykF* gene knockout *Escherichia coli* based on ^{13}C -labeling experiments together with measurements of enzyme activities and intracellular metabolite concentrations. *Appl Microbiol Biotechnol.* 2004;63:407–417.
 19. Kedar P, Colah R, Shimizu K. Proteomic investigation on the *pyk-F* gene knockout *Escherichia coli* for aromatic amino acid production. *Enzym Microb Tech.* 2007;41:455–465.
 20. Baba T, Ara T, Hasegawa M, Takai Y, Okumura Y, Baba M, Datsenko KA, Tomita M, Wanner BL, Mori H. Construction of *Escherichia coli* K-12 in-frame, single-gene knockout mutants: the Keio collection. *Mol Syst Biol.* 2006;2.
 21. Datsenko KA, Wanner BL. One-step inactivation of chromosomal genes in *Escherichia coli* K-12 using PCR products. *Proc Natl Acad Sci USA.* 2000;97:6640–6645.
 22. Ohashi Y, Hirayama A, Ishikawa T, Nakamura S, Shimizu K, Ueno Y, Tomita M, Soga T. Depiction of metabolome changes in histidine-starved *Escherichia coli* by CE-TOFMS. *Mol Biosyst.* 2008;4:135–147.
 23. Fischer E, Sauer U. Metabolic flux profiling of *Escherichia coli* mutants in central carbon metabolism using GC-MS. *Eur J Biochem.* 2003;270:880–891.
 24. Zhao J, Shimizu K. Metabolic flux analysis of *Escherichia coli* K12 grown on ^{13}C -labeled acetate and glucose using GC-MS and powerful flux calculation method. *J Biotechnol.* 2003;101:101–117.
 25. Van Winden WA, Wittmann C, Heinzle E, Heijnen JJ. Correcting mass isotopomer distributions for naturally occurring isotopes. *Biotechnol Bioeng.* 2002;80:477–479.
 26. Li M, Ho PY, Yao S, Shimizu K. Effect of *lpdA* gene knockout on the metabolism in *Escherichia coli* based on enzyme activities, intracellular metabolite concentrations and metabolic flux analysis by ^{13}C -labeling experiments. *J Biotechnol.* 2006;122:254–266.
 27. Fletcher R. Practical Methods of Optimization, Hoboken, NJ: Wiley; 2000.
 28. Edwards JS, Ibarra RU, Palsson BO. *In silico* predictions of *Escherichia coli* metabolic capabilities are consistent with experimental data. *Nat Biotechnol.* 2001;19:125–130.
 29. Varma A, Palsson BO. Stoichiometric flux balance models quantitatively predict growth and metabolic by-product secretion in wild-type *Escherichia coli* W3110. *Appl Environ Microbiol.* 1994;60:3724–3731.
 30. Price ND, Reed JL, Palsson BO. Genome-scale models of microbial cells: evaluating the consequences of constraints. *Nat Rev Microbiol.* 2004;2:886–897.
 31. Schuetz R, Kuepfer L, Sauer U. Systematic evaluation of objective functions for predicting intracellular fluxes in *Escherichia coli*. *Mol Syst Biol.* 2007;3:119.
 32. Dauner M, Bailey JE, Sauer U. Metabolic flux analysis with a comprehensive isotopomer model in *Bacillus subtilis*. *Biotechnol Bioeng.* 2001;76:144–156.
 33. Walsh K, Koshland DE Jr. Branch point control by the phosphorylation state of isocitrate dehydrogenase. A quantitative examination of fluxes during a regulatory transition. *J Biol Chem.* 1985;260:8430–8437.
 34. Veit A, Polen T, Wendisch VF. Global gene expression analysis of glucose overflow metabolism in *Escherichia coli* and reduction of aerobic acetate formation. *Appl Microbiol Biotechnol.* 2007;74:406–421.
 35. Cronan JE, Laporte D. Tricarboxylic acid cycle and glyoxylate bypass. In: Neihardt FC, Curtiss R, Ingraham JL, Lin ECC, Low KB, Magasanik B, Reznikoff WS, Riley M, Schaechter M, Umberger HE, Eds. *Escherichia coli and Salmonella: Cellular And Molecular Biology*, Washington, DC: ASM Press, 1996: 206–216.
 36. Wolfe AJ. The acetate switch. *Microbiol Mol Biol Rev.* 2005; 69:12–50.
 37. Kotlarz D, Buc H. Phosphofructokinases from *Escherichia coli*. *Methods Enzymol.* 1982;90:60–70.
 38. Yoshinaga T. Structural specificity of the allosteric inhibitor of phosphoenolpyruvate carboxylase of *Escherichia coli*. *J Biochem.* 1977;81:665–671.
 39. Ishii N, Nakahigashi K, Baba T, Robert M, Soga T, Kanai A, Hirasawa T, Naba M, Hirai K, Hoque A, Ho PY, Kakazu Y, Sugawara K, Igarashi S, Harada S, Masuda T, Sugiyama N, Togashi T, Hasegawa M, Takai Y, Yugi K, Arakawa K, Iwata N, Toya Y, Nakayama Y, Nishioka T, Shimizu K, Mori H, Tomita M. Multiple high-throughput analyses monitor the response of *E. coli* to perturbations. *Science.* 2007;316:593–597.
 40. Noraini AR, Shirai Y, Hassan MA, Shimizu K. Investigation on the metabolic regulation of *pgi* gene knockout *Escherichia coli* by enzyme activities and intracellular metabolite concentrations. *Mal J Microbiol.* 2006;2:24–31.
 41. Emmerling M, Dauner M, Ponti A, Fiaux J, Hochuli M, Szyperski T, Wüthrich K, Bailey JE, Sauer U. Metabolic flux responses to pyruvate kinase knockout in *Escherichia coli*. *J Bacteriol.* 2002;184:152–164.
 42. Yang C, Hua Q, Baba T, Mori H, Shimizu K. Analysis of *Escherichia coli* anaplerotic metabolism and its regulation mechanisms from the metabolic responses to altered dilution rates and phosphoenolpyruvate carboxykinase knockout. *Biotechnol Bioeng.* 2003;84:129–144.
 43. Wolf RE, Prather DM, Shea FM. Growth-rate-dependent alteration of 6-phosphogluconate dehydrogenase and glucose 6-phosphate dehydrogenase levels in *Escherichia coli* K-12. *J Bacteriol.* 1979;139:1093–1096.
 44. Peng L, Arauzo-Bravo MJ, Shimizu K. Metabolic flux analysis for a *ppc* mutant *Escherichia coli* based on ^{13}C -labelling experiments together with enzyme activity assays and intracellular metabolite measurements. *FEMS Microbiol Lett.* 2004;235:17–23.
 45. Canonaco F, Hess TA, Heri S, Wang T, Szyperski T, Sauer U. Metabolic flux response to phosphoglucose isomerase knock-out in *Escherichia coli* and impact of overexpression of the soluble transhydrogenase UdhA. *FEMS Microbiol Lett.* 2001;204:247–252.
 46. Rahman M, Hasan MR, Shimizu K. Growth phase-dependent changes in the expression of global regulatory genes and associated metabolic pathways in *Escherichia coli*. *Biotechnol Lett.* 2008;30:853–860.

APPENDIX

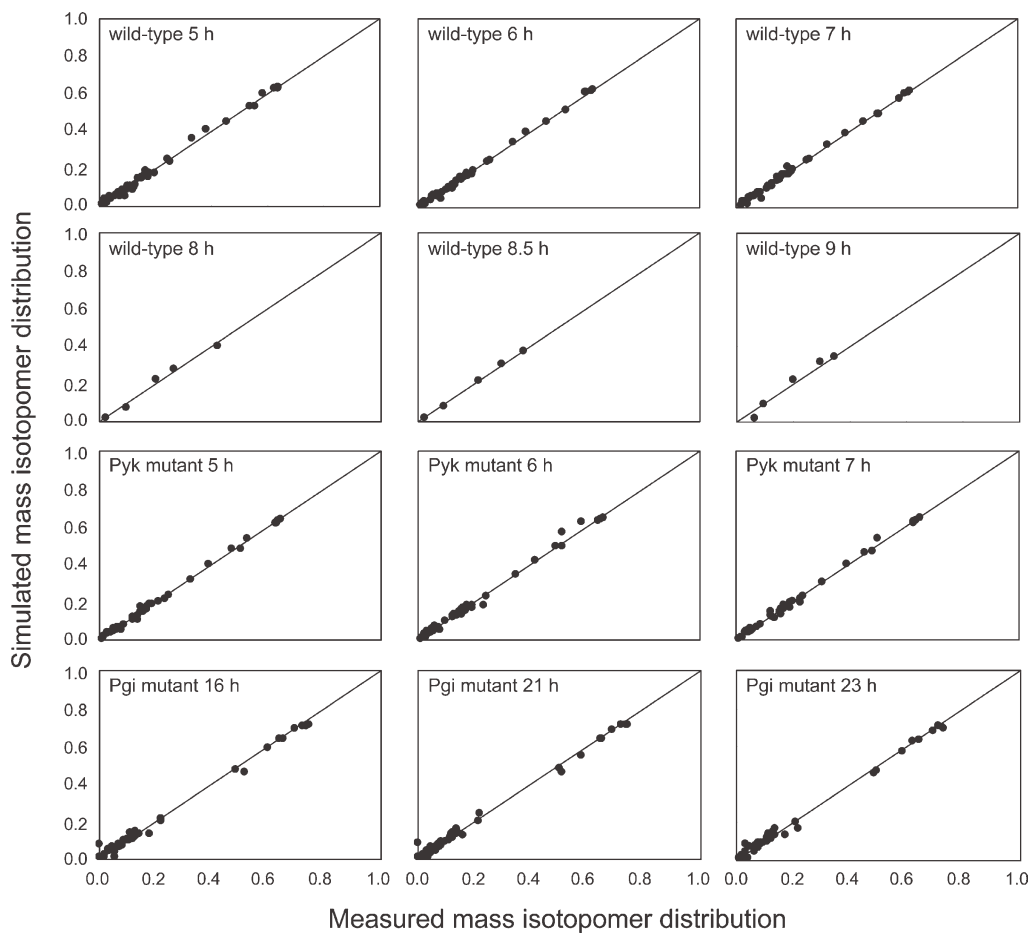


Figure A1. The comparisons between simulated and experimental data of wild-type, Pyk mutant and Pgi mutant.

All correlation coefficients were more than 0.99. The detailed values of the intracellular metabolite mass isotopomers of wild-type, Pyk mutant and Pgi mutant are summarized in Supporting Information Tables S-VIII, S-IX, and S-X, respectively.

Table A1. Abbreviation of metabolites

Abbreviation	Metabolite
3PG	3-phosphoglycerate
6PG	6-phosphogluconate
α KG	α -ketoglutarate
ACoA	acetyl-CoA
AcOHex	acetate extracellular
DHAP	dihydroxyacetone phosphate
E4P	erythrose-4-phosphate
F6P	fructose-6-phosphate
F16P	fructose-1,6-bisphosphate
FUM	fumarate
G3P	glyceraldehyde-3-phosphate
G6P	glucose-6-phosphate
GLCex	glucose extracellular
GOX	glyoxylate
ICT	isocitrate
MAL	malate
OAA	oxaloacetate
PEP	phosphoenolpyruvate
PYR	pyruvate
R5P	ribose-5-phosphate
Ru5P	ribulose-5-phosphate
S7P	sedoheptulose-7-phosphate
SUC	succinate
X5P	xylulose-5-phosphate

Table A2. Abbreviation of Reactions

Abbreviation	Reaction
6PGDH	6-phosphogluconate dehydrogenase
Ack	acetate kinase
Eno	enolase
Fba	fructose bisphosphate aldolase
G6PDH	glucose-6-phosphate dehydrogenase
ICDH	isocitrate dehydrogenase
Mez	malic enzyme
MDH	malate dehydrogenase
Pck	phosphoenolpyruvate carboxykinase
Pfk	phosphofructokinase
Pgi	phosphoglucose isomerase
Pgk	phosphoglycerate kinase
Ppc	phosphoenolpyruvate carboxylase
PTS	phosphotransferase system
Pyk	pyruvate kinase
Tal	transaldolase
Tk1	transketolase 1
Tk2	transketolase 2
Tpi	triosephosphate isomerase
Rpe	ribulose-5-phosphate epimerase
Rpi	ribulose-5-phosphate isomerase
SCS	succinyl-CoA synthetase

Manuscript received Sept. 19, 2009, and revision received Dec. 28, 2009.